J. Fluid Mech. (2010), *vol.* 663, *pp.* 148–159. © Cambridge University Press 2010
doi:10.1017/S0022112010003836

Model for unstable global modes in the rotating-disk boundary layer

J. J. HEALEY†

Department of Mathematics, Keele University, Keele, Staffordshire ST5 5BG, UK

(Received 10 May 2010; revised 12 July 2010; accepted 12 July 2010;
first published online 28 September 2010)

Recent simulations and experiments appear to show that the rotating-disk boundary layer is linearly globally stable despite the existence of local absolute instability. However, we argue that linear global instability can be created by local absolute instability at the edge of the disk. This argument is based on investigations of the linearized complex Ginzburg–Landau equation with weakly spatially varying coefficients to model the propagation of a wavepacket through a weakly inhomogeneous unstable medium. Therefore, this mechanism could operate in a variety of locally absolutely unstable flows. The corresponding nonlinear global mode has a front at the radius of onset of absolute instability when the disk edge is far from the front. This front moves radially outwards when the Reynolds number at the disk edge is reduced. It is shown that the laminar–turbulent transition front also behaves in this manner, possibly explaining the scatter in observed transitional Reynolds numbers.

Key words: absolute/convective instability, boundary layer stability

1. Introduction

This paper is concerned with the stability of the boundary layer that forms over a disk rotating in otherwise still fluid. Viscous stresses give an azimuthal velocity component to the flow, causing the fluid to spiral outwards, since there is no radial pressure gradient to constrain the fluid to follow circular paths. The disk thus acts as a centrifugal fan. The presence of both azimuthal and radial flow profiles gives it stability characteristics similar to those of three-dimensional boundary layers on swept wings (see Gregory, Stuart & Walker 1955), and this makes the rotating-disk boundary layer an important model for a variety of flows of practical interest; see the special issue 'Instabilities of flows due to rotating disks', vol. 57(3) of the *Journal of Engineering Mathematics*, see Healey (2007*a*).

We define a 'local' Reynolds number based on distance to the axis of rotation, r^*,

$$Re = (\Omega^*/\nu)^{1/2} r^*, \tag{1.1}$$

where Ω^* is the angular velocity of the disk, and ν is the kinematic viscosity of the fluid. This Reynolds number can also be viewed as the dimensionless radius scaled by the boundary-layer length scale $(\nu/\Omega^*)^{1/2}$. Stable laminar flow is observed for small Re. As Re increases the flow becomes unstable, and eventually becomes turbulent.

† Email address for correspondence: j.j.healey@maths.keele.ac.uk

https://doi.org/10.1017/S0022112010003836 Published online by Cambridge University Press

Authors	Re_t	Method
Gregory *et al.* (1955)	530	Visual, China-clay
Federov *et al.* (1976)	515	Visual, napthalene
Clarkson, Chin & Shacter (1980)	562	Visual, dye
Cobb & Saunders (1956)	490	Heat transfer
Chin & Litt (1972)	510	Mass transfer
Gregory & Walker (1960)	505	Pressure probe
Smith (1946)	557	Hot wire
Kobayashi, Kohama & Takamadate (1980)	500	Hot wire
Malik, Wilkinson & Orszag (1981)	520	Hot wire
Wilkinson & Malik (1985)	550	Hot wire
Lingwood (1996)	508	Hot wire
Othman & Corke (2006)	539	Hot wire

TABLE 1. Experimental Re_t, adapted from Malik *et al.* (1981). Different authors use different criteria for transition. Values given are for 'onset' of transition, or where 'significant nonlinear distortion' of waves first occurs. When authors report that transition occurs between a pair of measurement stations, the Re at the mid-point of the pair is given.

Table 1 shows the Reynolds numbers, Re_t, at which transition to turbulence has been observed in experiments.

The differences between Re_t might be attributable to the different surface roughness of different disks or to the sensitivity of the chosen measurement technique to the unsteady fluctuations that signal the onset of transition, e.g. a larger Re_t might imply that the disk surface was particularly smooth, or instead that the measurement, or visualization, technique was poor at detecting disturbances. To minimize this latter effect, we focus on the experiments in the lower part of the table, i.e. the 'modern' hot-wire results. However, even for these, the scatter is only a little less than for those in the upper part of the table.

In flows that are linearly stable, such as in a pipe, or only convectively unstable (CU), such as the Blasius boundary layer, Re_t is highly dependent on the disturbance environment, and can vary greatly from facility to facility. In contrast, globally unstable flows, which can support self-sustained oscillations, such as vortex shedding behind a cylinder, have a highly repeatable Reynolds number for the onset of instability. It was originally assumed that the rotating disk was CU, and that the scatter in Re_t was due to differing noise levels in different experiments, e.g. when Wilkinson & Malik (1985) used a highly polished disk they increased Re_t to above the value they had previously obtained in Malik *et al.* (1981).

However, Lingwood (1995) showed that the flow becomes locally absolutely unstable (AU) for $Re > 507$, and argued that this explains the relative repeatability of Re_t around this value. Her experiments (Lingwood 1996) show the trailing edge of wavepackets slowing down as they approach $Re = 507$ (see figure 1), apparently confirming the importance of local absolute instability (AI) in causing transition. Nonetheless, understanding of this problem changed again when Davies & Carpenter (2003) carried out direct numerical simulations of the linearized equations and found that wavepackets convect through the AU region without slowing down, showing that AI does not produce a linear global instability in this flow. In fact, the top most data points in figure 1(*b*) lie close to where the flow is becoming turbulent, and so may be affected by nonlinearity, as noted on p. 221 of Davies, Thomas & Carpenter (2007); without these points the claim that the trailing edge is slowing down as $Re \to 507$ is less compelling.

https://doi.org/10.1017/S0022112010003836 Published online by Cambridge University Press

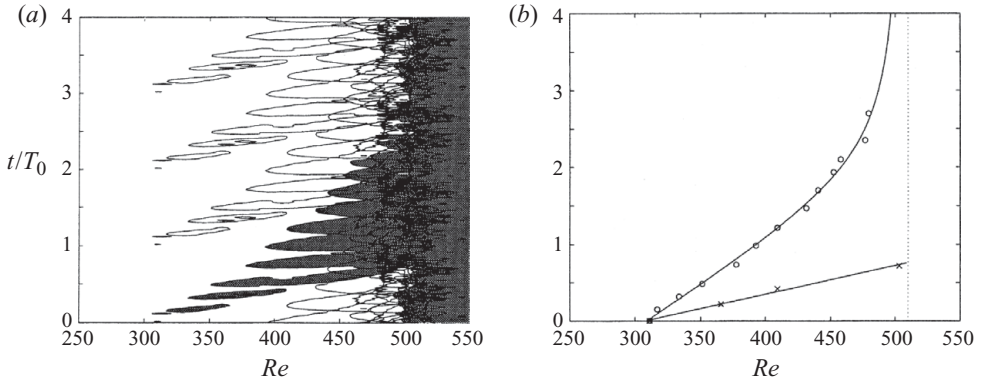


FIGURE 1. Experimental measurements of wavepackets in the rotating-disk boundary layer, reproduced from Lingwood (1996). The period of the disk is T_0. (*a*) Disturbance contours; (*b*) estimate of the leading and trailing edges of a wavepacket, the latter apparently asymptoting to the vertical dashed line at $Re = 507$, beyond which the flow is AU.

Subsequent work has shown how nonlinearity can create global instability: Pier (2003) has considered secondary AI of saturated nonlinear vortices, and Viaud, Serre & Chomaz (2008) have obtained a nonlinear global mode in simulations of a rotating channel flow (similar to rotating disk flow, but more tractable computationally). Othman & Corke (2006) produced an exceptionally clean rotating-disk flow experiment to demonstrate that sufficiently small amplitude disturbances are globally stable and can be followed well into the AU regime in agreement with Davies & Carpenter (2003).

However, in this paper a mechanism is proposed for linear global instability of the rotating-disk flow. A simple model is presented illustrating the mechanism and showing how it may explain the variability of the results seen in table 1.

2. Model for global instability

The linearized complex Ginzburg–Landau equation

$$\frac{\partial A}{\partial T} + U\frac{\partial A}{\partial X} = \mu A + \gamma \frac{\partial^2 A}{\partial X^2}, \tag{2.1}$$

with constant coefficients, describes the envelope of a wavepacket, $A(X, T)$, in a homogeneous medium when the instability is weak and the group velocity is slow. The parameter U characterizes the group velocity, $\mathrm{Re}(\mu)$ the instability, $\mathrm{Im}(\mu)$ the detuning between the carrier wave and the envelope and γ describes the spreading of the envelope (dispersion). A weakly inhomogeneous medium can be modelled by allowing the coefficients to depend weakly on X. We do not claim that all these restrictions necessarily apply in a strict asymptotic sense to the rotating-disk boundary layer near Re_t. Nonetheless, (2.1), with variable coefficients, has been widely used to understand issues of local and global instability (see Huerre 2000), and has been shown in Davies *et al.* (2007) to reproduce the stable global linear dynamics of the rotating-disk boundary layer seen in the direct numerical simulations of Davies & Carpenter (2003).

When waves on the rotating disk of fixed azimuthal wavenumber m are followed radially outwards, they are stable at small radii, become CU as the radius increases, and then, if m is large enough, they become AU. Therefore, we first consider a case

https://doi.org/10.1017/S0022112010003836 Published online by Cambridge University Press

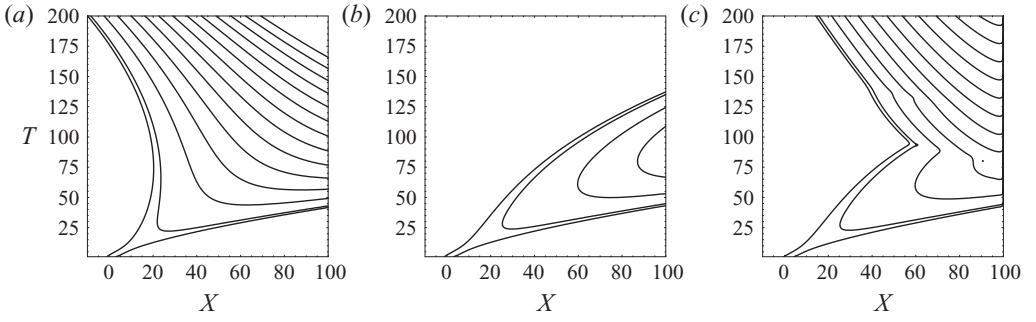


FIGURE 2. Contours of $|A|$ for an impulsive disturbance at $X = T = 0$ to (2.1) and (2.2) with $\epsilon = 0.01$ giving AI for $X > 25$. (*a*) and (*b*) are unbounded, $A \to 0$ as $X \to \pm\infty$, obtained using (31) of Hunt & Crighton (1991) where $\delta = 0$ in (*a*) giving global instability and $\delta = 2$ in (*b*) giving global decay. (*c*) is bounded with $A = 0$ at $X = 100$, and $\delta = 2$, obtained by numerical solution of (2.1), giving global instability excited by AI at the downstream boundary.

where μ increases linearly in X to model increasing instability as a wave propagates radially outwards and enters the AU region. For simplicity, let

$$\mu = \epsilon(1 + \mathrm{i}\delta)X, \quad U = \gamma = 1, \tag{2.2}$$

where $\epsilon \ll 1$ expresses the weakness of the spatial inhomogeneity, and δ describes the strength of the detuning. A more realistic X dependence is considered in § 2.3.

2.1. *Local stability and propagation*

The local stability properties, where μ is treated as a constant, with X acting as a parameter in (2.2), but as a variable in (2.1), are found by substituting $A = A_0 \exp \mathrm{i}(\alpha X - \omega T)$ into (2.1) to give the local dispersion relation

$$\omega = \alpha + \mathrm{i}(\mu - \alpha^2), \tag{2.3}$$

which is the leading-order result of a WKB theory. The AI frequency, i.e. ω at the pinch-point of Briggs' method (Briggs 1964), satisfying $\omega_\alpha = 0$, is given by

$$\omega_0 = \mathrm{i}(\mu - 1/4). \tag{2.4}$$

The flow is locally unstable when $\mathrm{Im}(\omega) > 0$ for some real α, and it is AU when $\mathrm{Im}(\omega_0) > 0$. Therefore, a flow modelled by (2.2) is locally stable for $X < 0$, CU for $0 < X < (4\epsilon)^{-1}$ and AU for $X > (4\epsilon)^{-1}$. The local stability properties are thus independent of the detuning parameter δ.

2.2. *Global stability properties*

However, the global stability properties depend sensitively on δ. Hunt & Crighton (1991) give an exact solution for an impulsive disturbance to (2.1) and (2.2) in an unbounded domain, and here we compare this global result with the local results of § 2.1. Substituting (2.2) into (31) of Hunt & Crighton (1991) as $T \to \infty$ for any fixed finite X gives

$$A \sim (4\pi T)^{-1/2} \exp[\epsilon^2(1 - \delta^2 + 2\mathrm{i}\delta)^2 T^3/12]. \tag{2.5}$$

Therefore, this flow is globally unstable for $\delta^2 < 1$ and globally stable for $\delta^2 > 1$. This stabilization by detuning, i.e. by the spatial variation of the local frequency, is called 'phase-mixing' and was reported in a convection problem on pp. 42–43 of Soward (1977). Figure 2(*a*) shows an example with zero detuning, $\delta = 0$, giving global

https://doi.org/10.1017/S0022112010003836 Published online by Cambridge University Press

instability, as expected from the local results since there is AI. Figure 2(*b*) shows an example with $\delta = 2$ giving a globally stable flow, despite the existence of AI. This latter case reflects the situation for the rotating-disk boundary layer; see Davies *et al.* (2007).

In fact, this behaviour is a consequence of having the disturbance evolve in an infinite domain. Of course, physical problems have a finite domain. The key point of this paper is that making the domain finite, e.g. to model the behaviour of a finite-radius rotating disk, can have an important destabilizing effect on the global stability properties. We illustrate this effect by imposing the downstream boundary condition $A(h, T) = 0$ on (2.1). Substituting $A = \psi(X)\exp(-\mathrm{i}\omega_G T)$ into (2.1) and (2.2) gives

$$\psi'' - \psi + [\epsilon(1 + \mathrm{i}\delta)X + \mathrm{i}\omega_G]\psi = 0, \tag{2.6}$$

and the boundary conditions $\psi \to 0$ as $X \to -\infty$ and $\psi(h) = 0$ give an eigenvalue problem for the global frequency, ω_G. Solving (2.6) in terms of Airy functions gives

$$\omega_G = \mathrm{i}\big[\epsilon(1 + \mathrm{i}\delta)h - 1/4 + \epsilon^{2/3}(1 + \mathrm{i}\delta)^{2/3} b_j\big], \tag{2.7}$$

where $\mathrm{Ai}(b_j) = 0$, i.e. $b_j \approx -2.34, -4.09, \ldots$. A similar solution was found by Chomaz, Huerre & Redekopp (1987) but instead for flow downstream of a boundary modelling a wake flow. We can rewrite (2.7) using (2.2) and (2.4) as

$$\omega_G = \omega_0(h) + \mathrm{i}\epsilon^{2/3}(1 + \mathrm{i}\delta)^{2/3} b_j, \tag{2.8}$$

where $\omega_0(h)$ is the AI frequency (2.4) evaluated at the downstream boundary $X = h$.

Figure 2(*c*) shows an impulsive disturbance in a flow that is globally stable when unbounded. The disturbance propagates through the AU region exactly as in the unbounded case shown in figure 2(*b*), until it reaches the downstream boundary, where it excites an unstable global mode, with growth rate correctly predicted by (2.8).

Thus, restriction to a finite domain can create global instability if the boundary is situated in a region of AI even when the unbounded problem is globally stable. The choice of boundary condition only affects the correction term in (2.8).

2.3. *Relation to previous global mode theories and rotating-disk local stability results*

The model (2.2), with local instability increasing arbitrarily in the downstream direction, does not apply over larger extents of the rotating disk. An AU wave is only AU over a finite range of radii, r (i.e. finite range of Re), and reverts to CU as the radius (Re) increases; see figure 3(*a*). For example, the mode with azimuthal wavenumber $m = 68$ is only AU for $507 < Re < 1580$, and the absolute growth rate and frequency vary approximately quadratically over this range of radius (Re) (see figure 3*b*), which motivates the investigation of the Ginzburg–Landau equation with a quadratically varying instability coefficient below. This figure also shows that the absolute frequency, $\mathrm{Re}(Re\,\omega_0)$, varies much more strongly with radius than the absolute growth rate, $\mathrm{Im}(Re\,\omega_0)$. Therefore, detuning is strong for this flow and exerts a strong stabilizing influence, as argued by Davies *et al.* (2007). The strength of the detuning also implies that any saddle $\partial(Re\,\omega_0)/\partial Re = 0$, which controls the linear global mode in an unbounded domain (see Soward & Jones 1983; Chomaz, Huerre & Redekopp 1991, and below), lies far from the real Re axis in the complex Re plane, and preliminary results confirm that for any such saddle, $\mathrm{Im}(Re\,\omega_0) < 0$, predicting that linear global modes in an unbounded domain are stable for a wide range of m.

https://doi.org/10.1017/S0022112010003836 Published online by Cambridge University Press

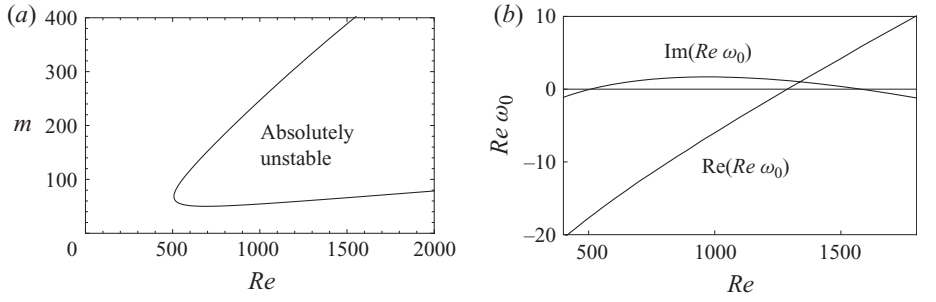


FIGURE 3. Numerical parallel-flow stability solutions for von Kármán's similarity solution for rotating-disk flow. (*a*) Range of AI. (*b*) Variation of the local absolute frequency, $Re\,\omega_0$, with dimensionless radius, Re, for azimuthal wavenumber $m = 68$.

The parallel-flow stability equations for the rotating-disk flow, and the numerical method for their solution (based on Chebyshev polynomials), are presented in Healey (2004), and the results in figure 3 were obtained using the same code.

A simple model for wavepackets travelling through a finite region of AI is

$$\mu = \mu_0 + \epsilon\mu_1 X + \epsilon^2\mu_2 X^2, \quad U = \gamma = 1, \tag{2.9}$$

with $\mathrm{Re}(\mu_2) < 0$ to give a maximum in the instability parameter, as in figure 3(*b*). Global modes are sought by substituting $A = \exp(-\mathrm{i}\omega_G T)\psi(X)$ and (2.9) into (2.1) to give

$$\psi'' - \psi' + [\mu_0 + \epsilon\mu_1 X + \epsilon^2\mu_2 X^2 + \mathrm{i}\omega_G]\psi = 0, \tag{2.10}$$

which can be transformed into Hermite's equation,

$$y'' - 2xy' + 2ny = 0, \tag{2.11}$$

by a change of variables of the form $\psi(X) = y(x)\exp(q_0x^2 + q_1x)$, $X = q_2x + q_3$, where

$$\omega_G = \mathrm{i}\left[\mu_0 - \frac{\mu_1^2}{4\mu_2} - 1/4 - \epsilon\sqrt{-\mu_2}(2n+1)\right] = \omega_0(X_S) - \mathrm{i}\epsilon\sqrt{-\mu_2}(2n+1) \tag{2.12}$$

and X_S is the location in the complex X plane of the saddle point, $\partial\omega_0/\partial X = 0$, as discussed above, and as found by Chomaz *et al.* (1987). This is why, to leading order, the global mode frequency is given by the AI frequency at this saddle point. The eigenvalue n of (2.11) is determined by applying homogeneous boundary conditions.

The global frequency, ω_G, given by (2.12) only depends weakly on n, so it appears that ω_G only depends weakly on the boundary conditions, contrary to the assertion in § 2.2 that the boundaries can strongly affect the global dynamics. This claim was deduced from a model with no saddle point X_S, and no global modes when the domain is unbounded. Nonetheless, there are situations when the boundaries do strongly affect the global modes for (2.9), and the rotating-disk boundary layer is such a case.

The general solution to (2.11) can be written as

$$y = C_1 H_n(x) + C_2\,{}_1F_1(-n/2, 1/2, x^2), \tag{2.13}$$

where H_n is the Hermite function, ${}_1F_1$ is the confluent hypergeometric function and C_1 and C_2 are arbitrary constants. Both of these functions grow exponentially for large $|x|$, unless $n = 0, 1, 2, 3, \ldots$, in which case H_n only grows algebraically (giving

https://doi.org/10.1017/S0022112010003836 Published online by Cambridge University Press

Hermite polynomials). The eigenvalues for the unbounded case, where $\psi \to 0$ as $X \to \pm\infty$, are therefore $n = 0, 1, 2, 3, \ldots$, and $C_2 = 0$.

Now impose the downstream boundary condition $\psi(h) = 0$, i.e. $y(h_0) = 0$ (where $h = q_2 h_0 + q_3$ from the change of variables used to derive (2.11)), which is satisfied by

$$C_1/C_2 = -{}_1F_1\big(-n/2, 1/2, h_0^2\big)/H_n(h_0). \tag{2.14}$$

The eigenrelation for n is then obtained by removing the exponential growth of y as $x \to -\infty$. Examination of the asymptotic forms of $H_n(x)$ and ${}_1F_1(-n/2, 1/2, x^2)$ for large negative x, and $n \neq 0, 1, 2, 3, \ldots$, gives the global mode eigenrelation

$$0 = \pi H_n(h_0) + \Gamma(-n/2)\Gamma(n+1)\sin(n\pi)\,{}_1F_1\big(-n/2, 1/2, h_0^2\big), \tag{2.15}$$

to be solved for n for a given h_0. Note that h_0 is real when the coefficients (2.9) are real, i.e. when there is no detuning, and that $h_0 > 0$ ($h_0 < 0$) corresponds to placing the boundary downstream (upstream) of the position of maximum local instability.

The following asymptotic approximations to (2.15) are obtained when h_0 is real:

$$n \sim \frac{h_0 \mathrm{e}^{-h_0^2}}{\sqrt{\pi}}, \quad 1 + \frac{2h_0^3 \mathrm{e}^{-h_0^2}}{\sqrt{\pi}}, \quad 2 + \frac{2h_0^5 \mathrm{e}^{-h_0^2}}{\sqrt{\pi}}, \ldots \quad \text{when } h_0 \gg 1, \tag{2.16a}$$

$$n \sim \frac{h_0^2}{2} - 2^{-1/3} b_j (-h_0)^{2/3} - \frac{1}{2} \quad \text{when } -h_0 \gg 1,\ n \gg 1 \text{ and } h_0^2 \sim 1 + 2n, \tag{2.16b}$$

where $\mathrm{Ai}(b_j) = 0$; (2.16b) was obtained by re-expressing $H_n(x)$ in terms of the two independent solutions of Kummer's equation, and using, in particular, (13.5.19) of Abramowitz & Stegun (1964), which approximates a hypergeometric function by Airy functions.

The non-negative integer n solutions for the unbounded global modes are recovered in (2.16a). In this range the boundary only creates an exponentially small correction to the unbounded problem. However, when $-h_0 \gg 1$ we find that $n \gg 1$ and this allows the boundary-influenced 'correction' in (2.12) to become large, so that the global mode frequency is no longer necessarily determined by the AI frequency at the saddle point, X_S. In fact, substituting (2.16b) into (2.12), and converting from h_0 back to h, gives

$$\omega_G = \mathrm{i}\big[\mu_0 + \epsilon\mu_1 h + \epsilon^2\mu_2 h^2 - 1/4 + b_j \epsilon^{2/3}(\mu_1 + 2\epsilon\mu_2 h)^{2/3}\big]. \tag{2.17}$$

This result is precisely in the form of (2.7) when (2.9) is linearized about $X = h$, and shows that when the boundary is far enough upstream of the position of maximum instability, the case of linear variation of the instability parameter (2.2) is the correct asymptotic limit. Figure 4(a) shows that (2.16b) and (2.17) (or (2.8)) give a good approximation even when the boundary is only a little upstream of the position of maximum instability, and that the boundary-triggered global modes given by (2.16b) evolve smoothly into the unbounded global modes given by (2.16a) as the boundary moves downstream.

However, there are qualitative differences in the case of complex coefficients shown in figure 4(b). In this example, the unbounded global modes are stable, but the AI generates global instability when the boundary lies within a finite range. The 'upstream' asymptotic for the boundary-triggered mode (2.16b) turns out to be accurate both upstream and downstream of the position of maximum local instability. The boundary-triggered modes and the unbounded modes are no longer continuations of one another, but form distinct branches of the global dispersion relation.

https://doi.org/10.1017/S0022112010003836 Published online by Cambridge University Press

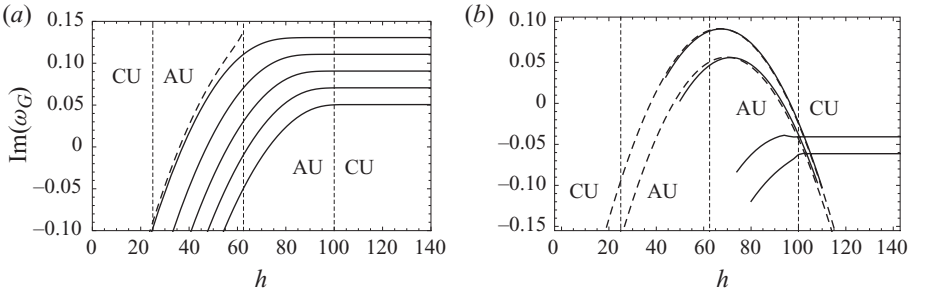


FIGURE 4. Global-mode growth-rate dependence on the position of the downstream boundary for $\epsilon = 0.01$. Solid lines are roots of (2.15); dashed lines are (2.16*b*). (*a*) Real coefficients, $\mu_0 = 0$, $\mu_1 = 5/4$, $\mu_2 = -1$; (*b*) with detuning, $\mu_0 = 0$, $\mu_1 = 5/4 + 0.3\mathrm{i}$, $\mu_2 = -1 + 0.5\mathrm{i}$ (giving complex h_0). In both cases the vertical dotted lines show the transitions between CU and AU regions, and also the location of the strongest AI.

The case shown in figure 4(*b*) is applicable to rotating-disk flow and, further, because azimuthal wavenumbers generate overlapping ranges of AI, there will be global instability whenever the Reynolds number at the edge of the disk is sufficiently greater than 507.

Davies & Carpenter (2003) carried out direct numerical simulations for linearized $m = 67$ modes, and they also encountered upstream propagation triggered by the downstream condition consistent with our results in figure 2(*c*). However, this phenomenon was regarded as a spurious numerical artefact, and so simulations were stopped before upstream propagation from the outflow condition reached the region of interest (see their p. 299). Nonetheless, figure 4(*b*) suggests that if the domain is large enough, then this upstream propagation can be avoided.

2.4. *Nonlinear global modes*

The growth of the global mode shown in figure 2(*c*) is expected to be eventually limited by nonlinearity. The simplest model for this nonlinear stabilization is

$$\frac{\partial A}{\partial T} + U\frac{\partial A}{\partial X} = \mu A + \gamma\frac{\partial^2 A}{\partial X^2} - |A|^2 A. \tag{2.18}$$

Figure 5 shows that a steep-fronted nonlinear global mode is produced with the front situated at the CU–AU transition location, $X_{CA} = 25$, as first seen by Meunier *et al.* (1997) and Pier *et al.* (1998). This is in qualitative agreement with Lingwood's wavepacket experiment on the rotating disk shown in figure 1, and with the direct numerical simulations of Viaud *et al.* (2008). The presence of detuning does not affect the position of this primary front, but can create a secondary front riding on the fully nonlinear solution, e.g. at $X \approx 70$ in figure 5(*b*). If h is increased sufficiently then tertiary, quaternary and additional fronts are seen further downstream and spatio-temporal chaos is often observed.

Figure 6(*a*) shows that the position of the front is fixed at X_{CA} when the boundary is far enough downstream, while figure 6(*b*) shows that the front moves downstream a little when the boundary moves upstream and approaches the location where the linear global mode is stabilized at $h_c = 35.85$ ($h_c > X_{CA} = 25$, due to the $O(\epsilon^{2/3})$ correction in (2.8)).

The qualitative behaviour of the front location, X_f, (defined e.g. by $A(X_f, T) = 0.05$) is shown in figure 7(*a*). The important trends are that $X_f \to X_{CA}$ as $h \to \infty$, and that

https://doi.org/10.1017/S0022112010003836 Published online by Cambridge University Press

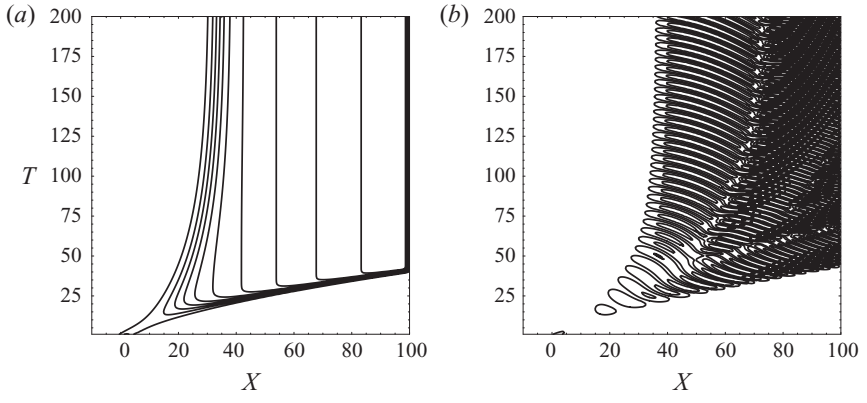


FIGURE 5. Contours of Re(A) for an impulsive disturbance at $X = T = 0$ to (2.2), (2.18) with $\epsilon = 0.01$, giving AI for $X > 25$, and downstream boundary condition $A(100, T) = 0$, obtained numerically. (a) $\delta = 0$ gives a stable steady nonlinear solution; (b) $\delta = 2$ gives a nonlinear solution that is unstable to secondary instabilities.

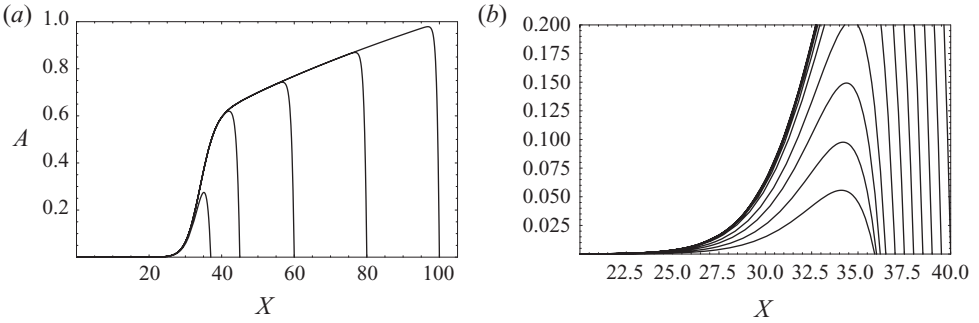


FIGURE 6. Dependence of the front on the location of the downstream boundary, $X = h$, from numerical solutions of (2.18) with (2.2) and $\epsilon = 0.01$, $\delta = 0$ (the presence of detuning, $\delta \neq 0$, does not affect the position of the front, but can lead to a complicated unsteady solution instead (see figure 5), so for simplicity we use $\delta = 0$ here). (a) $h = 37, 45, 60, 80, 100$; (b) $h = 35.9, 36, 36.2, 36.5, 37, 37.5, 38, 38.5, 39, 39.5, 40$.

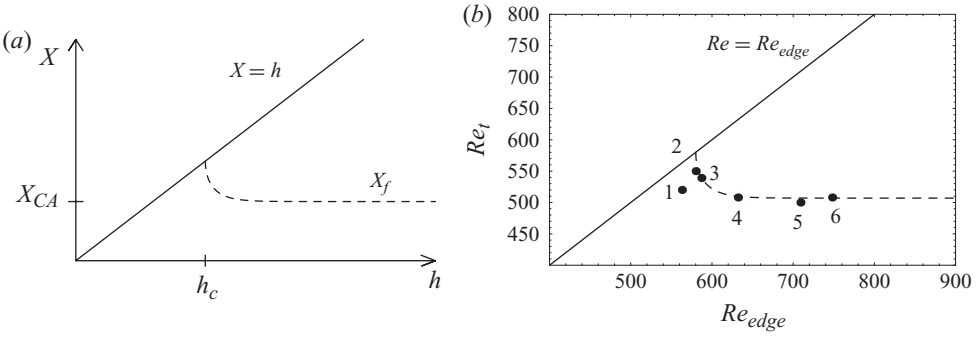


FIGURE 7. (a) Qualitative behaviour of the position of the front, X_f, as a function of position of downstream boundary, h, deduced from figure 6. (b) Dependence of Re_t on the Reynolds number at the edge of the disk, Re_{edge}, in the experiments (solid disks) in the lower part of table 1: 1 is Malik *et al.* (1981), 2 is Wilkinson & Malik (1985), 3 is Othman & Corke (2006), 4 and 6 are Lingwood (1996), 5 is Kobayashi *et al.* (1980). The qualitative behaviour of the front in the global mode theory (dashed line) is also shown.

https://doi.org/10.1017/S0022112010003836 Published online by Cambridge University Press

$X_f \to h_c > X_{CA}$ as $h \to h_c$. If the transition to turbulence is related to the appearance of a steep-fronted nonlinear global mode, then Re_t should depend in a similar manner on the Reynolds number at the edge of the disk, Re_{edge}. Figure 7(b) shows that the experiments do indeed follow this qualitative behaviour, in that all the experiments with Re_{edge} significantly larger than Re_t show transition close to $Re = 507 \equiv X_{CA}$, and the experiments with larger Re_t all had transition very close to the edge of the disk.

To make a quantitative prediction for the dashed curve in figure 7(b), it would be necessary to consider the basic flow near, and beyond, the edge of the disk, because the global mode theory predicts that the intercept of this curve with the downstream boundary (disk edge) depends on the nature of the downstream boundary, i.e. h_c depends on the boundary condition via the correction term in (2.8), where $\mathrm{Im}(\omega_G(h_c)) = 0$. Furthermore, rather than applying a boundary condition at the edge of the disk, it may be more appropriate to match the global mode to a solution existing in the flow off the edge of the disk. Finally, the behaviour of the curve near this intercept is controlled by nonlinearity, and could be obtained using weakly nonlinear theory when $h \approx h_c$ and the growth rate of the global mode is weak.

The global mode front represents the largest Re_t obtainable in a 'clean' experiment, and so is an upper bound on transition. The point marked '1' may be a case where transition was triggered by convective instabilities. When this rotating disk was polished, the result marked '2' was obtained, which was taken at a higher angular velocity. It would be consistent with the global mode theory to suggest that perhaps running the polished disk at the speed used in '1' leads to laminar flow over the entire disk, and that it was rotated a little faster in '2' to create transition just inside the edge of the disk.

3. Conclusions

A mechanism for producing linear global instability in the rotating-disk boundary layer has been proposed. When the spatial variation of the AI frequency (the detuning) is strong enough, it causes a flow to be globally stable, despite the existence of AI, and this is the case for the rotating-disk boundary layer. However, we have shown that this only applies to infinite rotating disks, and that linear global instability can, nonetheless, occur in flow on a finite rotating disk. At leading order, the global instability growth rate and frequency are given by the AI at the edge of the disk; see (2.8).

Creation of global instability by application of a downstream boundary condition has been seen before by Wang & Rusak (1996) in a model for vortex breakdown, where the local flow was only neutrally stable. The effect of a wavepacket striking a downstream boundary in a homogeneous flow in a finite domain was studied in Tobias, Proctor & Knobloch (1998), and our study can be viewed as a generalization of this work to inhomogeneous flow. Our study also complements recent work showing how boundaries parallel to the flow can destabilize AI (see Healey 2007*b*, 2008, 2009). The global instability in the present study is created by AI at the downstream boundary, which gives the boundary an upstream influence. In the cases of AI enhanced by a lateral boundary, it is the presence of a novel convective instability in the cross-stream direction (see Healey 2006) that allows the lateral boundary to influence stability through setting up standing modes connecting the lateral boundary and the shear layer. It will be interesting to see how combinations of lateral and downstream boundaries affect global instability.

https://doi.org/10.1017/S0022112010003836 Published online by Cambridge University Press

A simple nonlinear model shows that a front appears at the onset of AI when the disk edge is far from the front, and that the front moves downstream a little when the disk edge approaches the front (a higher-order effect). The Reynolds number at the edge of the disk, Re_{edge}, is the only global parameter for a rotating-disk experiment, so it is surprising that previous authors have not investigated whether Re_t in different experiments might be correlated to Re_{edge}. We find that they are correlated, and that, furthermore, they follow the same trends predicted by our nonlinear global mode theory. It is hoped that these findings can lead to a detailed explanation for the scatter in Re_t seen in table 1.

REFERENCES

Abramowitz, M. & Stegun, J. A. 1964 *Handbook of Mathematical Functions*. National Bureau of Standards.

Briggs, R. J. 1964 *Electron–Stream Interaction with Plasmas*. MIT Press.

Chin, D. & Litt, M. 1972 An electrochemical study of flow instability on a rotating disk. *J. Fluid Mech.* **54**, 613–625.

Chomaz, J. M., Huerre, P. & Redekopp, L. G. 1987 Models of hydrodynamic resonances in separated shear flows. In *Proceedings of the 6th Symposium on Turbulent Shear Flows Toulouse, France*, pp. 119–144.

Chomaz, J. M., Huerre, P. & Redekopp, L. G. 1991 A frequency selection criterion in spatially developing flows. *Stud. Appl. Math.* **84**, 119–144.

Clarkson, M. H., Chin, S. C. & Shacter, P. 1980 Flow visualizations of inflexional instabilities on a rotating disk. *AIAA Paper* 80-0279.

Cobb, E. C. & Saunders, O. A. 1956 Heat transfer from a rotating disk. *Proc. R. Soc. Lond.* A **236**, 343–351.

Davies, C. & Carpenter, P. W. 2003 Global behaviour corresponding to the absolute instability of the rotating-disk boundary layer. *J. Fluid Mech.* **486**, 287–329.

Davies, C., Thomas, C. & Carpenter, P. W. 2007 Global stability of the rotating-disc boundary layer. *J. Engng Math.* **57**, 219–236.

Federov, B. I., Plavnik, G. Z., Prokhorov, I. V. & Zhukhovitskii, L. G. 1976 Transitional flow conditions on a rotating disk. *J. Engng Phys.* **31**, 1448–1453.

Gregory, N., Stuart, J. T. & Walker, W. S. 1955 On the stability of three-dimensional boundary layers with application to the flow due to a rotating disk. *Phil. Trans. R. Soc. Lond.* A **248**, 155–199.

Gregory, N. & Walker, W. S. 1960 Experiments on the effect of suction on the flow due to a rotating disk. *J. Fluid Mech.* **9**, 225–234.

Healey, J. J. 2004 On the relation between the viscous and inviscid absolute instabilities of the rotating-disk boundary layer. *J. Fluid Mech.* **511**, 179–199.

Healey, J. J. 2006 A new convective instability of the rotating-disk boundary layer with growth normal to disk. *J. Fluid Mech.* **560**, 279–310.

Healey, J. J. 2007*a* Instabilities of flows due to rotating disks: preface. *J. Engng Math.* **57**, 199–204.

Healey, J. J. 2007*b* Enhancing the absolute instability of a boundary layer by adding a far away plate. *J. Fluid Mech.* **579**, 29–61.

Healey, J. J. 2008 Inviscid axisymmetric absolute instability of swirling jets. *J. Fluid Mech.* **613**, 1–33.

Healey, J. J. 2009 Destabilizing effects of confinement on homogeneous mixing layers. *J. Fluid Mech.* **623**, 241–271.

Huerre, P. 2000 Open shear flow instabilities. In *Perspectives in Fluid Dynamics* (ed. G. K. Batchelor, H. K. Moffatt & M. G. Worster), pp. 159–229. Cambridge University Press.

Hunt, R. E. & Crighton, D. G. 1991 Instability of flows in spatially developing media. *Proc. R. Soc. Lond.* A **435**, 109–128.

Kobayashi, R., Kohama, Y. & Takamadate, Ch. 1980 Spiral vortices in boundary layer transition regime on a rotating disk. *Acta Mech.* **35**, 71–82.

https://doi.org/10.1017/S0022112010003836 Published online by Cambridge University Press

Lingwood, R. J. 1995 Absolute instability of the boundary layer on a rotating disk. *J. Fluid Mech.* **299**, 17–33.

Lingwood, R. J. 1996 An experimental study of absolute instability of the rotating-disk boundary layer flow. *J. Fluid Mech.* **314**, 373–405.

Malik, M. R., Wilkinson, S. P. & Orszag, S. A. 1981 Instability and transition in rotating disk flow. *AIAA J.* **19**, 1131–1138.

Meunier, N., Proctor, M. R. E., Sokoloff, D. D., Soward, A. M. & Tobias, S. M. 1997 Asymptotic properties of a nonlinear $\alpha\omega$-dynamo wave: period, amplitude and latitude dependence. *Geophys. Astrophys. Fluid Dyn.* **86**, 249–285.

Othman, H. & Corke, T. C. 2006 Experimental investigation of absolute instability of a rotating-disk boundary layer. *J. Fluid Mech.* **565**, 63–94.

Pier, B. 2003 Finite-amplitude crossflow vortices, secondary instability in the rotating-disk boundary layer. *J. Fluid Mech.* **487**, 315–343.

Pier, B., Huerre, P., Chomaz, J. M. & Couairon, A. 1998 Steep nonlinear global modes in spatially developing media. *Phys. Fluids* **10**, 2433–2435.

Smith, N. H. 1946 Exploratory investigation of laminar boundary layer oscillations on a rotating disk. *NACA Tech. Note* 1227.

Soward, A. M. 1977 On the finite amplitude thermal instability of a rapidly rotating fluid sphere. *Geophys. Astrophys. Fluid Dyn.* **9**, 19–74.

Soward, A. M. & Jones, C. A. 1983 The linear stability of the flow in the narrow gap between two concentric rotating spheres. *Q. J. Mech. Appl. Math.* **36**, 19–42.

Tobias, S. M., Proctor, M. R. E. & Knobloch, E. 1998 Convective and absolute instabilities of fluid flows in finite geometries. *Physica* D **113**, 43–72.

Viaud, B., Serre, E. & Chomaz, J. M. 2008 The elephant mode between two rotating disks. *J. Fluid Mech.* **598**, 451–464.

Wang, S. & Rusak, Z. 1996 On the stability of an axisymmetric rotating flow in a pipe. *Phys. Fluids* **8**, 1007–1016.

Wilkinson, S. P. & Malik, M. R. 1985 Stability experiments in the flow over a rotating disk flow. *AIAA J.* **23**, 588–595.

https://doi.org/10.1017/S0022112010003836 Published online by Cambridge University Press